Article

Temporal Proteomic and Lipidomic Profiles of Cerulein-Induced Acute Pancreatitis Reveal Novel Insights for Metabolic Alterations in the Disease Pathogenesis

Rui Wang, Yiqin Wang, Yiran Tao, Liqiang Hu, Qi Qiu, Qianlun Pu, Juqin Yang, Shisheng Wang, Yan Huang, Xiaoting Chen, Ping Zhu, Hao Yang, Qing Xia, and Dan Du*

Cite This: ACS Omega 2023, 8, 12310−12326

Read Online

ACCESS | Metrics & More | Article Recommendations | Supporting Information

ABSTRACT: The pathophysiological mechanisms of acute pancreatitis (AP) are complex and have remained a mystery to date, but metabolism is gradually recognized as an important driver of AP onset and development. We used a cerulein-induced AP mouse model to conduct liquid chromatography−mass spectrometry (LC−MS/MS)-based time-course proteomics and lipidomics in order to better understand the underlying metabolic alterations linked with AP. Results showed that a series of significant changes in proteins over time with a boost in expression were enriched in lipase activity, lipoprotein, and lipids absorption and transport regulation. Furthermore, 16 proteins associated with lipid metabolism and signaling pathways together with the whole lipid species changing profile led to the vital identification of changing law in glycerides, phosphoglycerides, and free fatty acids. In addition to lipid metabolism and regulation-associated proteins, several digestive enzymes and adaptive anti-trypsin, stress response, and energy metabolism-related proteins showed an increment in abundance. Notably, central carbon and branched chain amino acid metabolism were enhanced during 0−24 h from the first cerulein stimulation. Taken together, this integrated proteomics and lipidomics revealed a novel metabolic insight into metabolites transforming rules that might be relevant to their function and drug targets investigation. (Created with Biorender.com.)
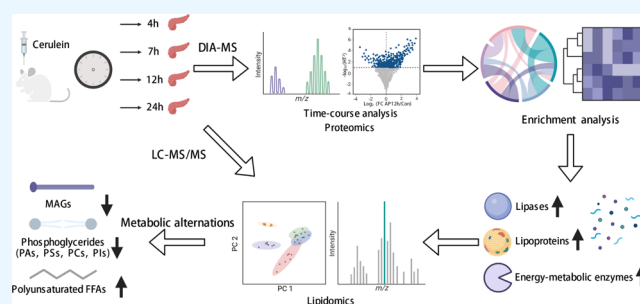
INTRODUCTION

Acute pancreatitis (AP) is a pancreatic inflammatory illness that manifests suddenly with excruciating abdominal pain and has the potential to be life-threatening.[1] The three main etiologies are biliary pathologies, alcohol use, and hyper-triglyceridemia (HTG).[1] Effective treatments for AP remain scarce despite improvements in diagnosis and management because of our incomplete understanding of the disease mechanisms.[2] Based on limited experimental AP, significant progress has been made in revealing the mechanisms of premature digestive enzyme activation,[3] intracellular calcium overload,[4] endoplasmic reticulum (ER) stress,[5] the inflammatory cascade,[6] autophagy dysfunction and mitochondrial failure,[7] and several agents are already in development.[8,9] The exact pathophysiological mechanisms of AP remain a mystery. Omics data are required to address the heterogeneity and narrow the gap between preclinical and clinical translations.[10,11]

In recent years, the metabolic disorder has become more and more significant in the onset and progression of AP.[12] When AP occurs, it results in severe digestive system problems, including the production of excessive amounts of digestive juices that decompose protein, carbohydrates, and fat.[13] This situation is linked to a disruption in the homeostatic metabolism of sugars, amino acids, organic acids, and lipids in mammalian cells and gut microbes.[14] In addition to serving as regulators of sensing and signaling, these dynamically altering metabolites may also be responsible for the disease's second attack.[15] Thus, directly interfering with metabolic processes may be a substitute and more effective method of identifying new therapeutic targets.[16] Based on a unique time-course metabolomics investigation in a cerulein (CER)-induced AP model, our previous study[17] identified several continuously interrupted pathways and hub metabolites. The utilization of multiple omics will mainly compensate for the bottlenecks of metabolic mechanisms and protein−metabolites interactions that are challenging to resolve by single omics due to the complexity and significance of the pancreas as an exocrine organ.[18]

Systematic proteomic studies have considerably accelerated the hunt for biomarkers and revealed disease mechanisms in earlier pancreatic disease research.[19−24] Particularly, the advent of high-throughput proteomics based on LC−MS/MS has elucidated hundreds of divergent proteins and effectively addressed the workflow issue of pancreatic protein degradation.[25] Numerous important up- and down-regulated proteins associated with inflammation, digestive enzymes, metabolism, signal transduction, and other processes were identified by these quantitative proteomic analyses in conjunction with functional annotations.[26−31] However, we were unable to fully comprehend the pathophysiology of AP due to the inconsistent protein changes obtained from CER[26−28,32] or sodium taurocholate (NaT)-induced AP rats[29] at a single time point. In this regard, an edematous AP model with multiple time points and simple replication helps us grasp the dynamics of protein levels. Additionally, lipids serve as enzyme substrates, govern protein structures, and modulate their structures, all of which have an impact on cellular processes.[33] Unsaturated fatty acids have been shown to have harmful effects on acinar cells or AP mice.[34] Unfortunately, there have not been any broad-spectrum lipidomic studies on animal models until now. The potential role of other lipids in AP is unknown to us.

Here, we proposed a data-independent acquisition mass spectrometry (DIA-MS) method with higher protein coverage applied to the CER-AP, 3803 proteins were relative quantified in all pancreatic samples and 171 significantly altered proteins were disclosed across all time points. Subsequent function analysis showed impaired lipid transport, regulation, and metabolism, which was further demonstrated by a broad-spectrum, targeted lipidomic profiling and the elucidation of lipid species interconversions in the pancreas. Lastly, we integrated the altered pancreatic proteomes involved in the pathways for the amino acids and center carbon metabolism revealed by KEGG analysis and mapped their metabolic dynamics profiling during the early and recovery stages of AP. It is worth mentioning that the results of the integrated temporal proteomics and lipidomics will give us new insights into biological processes (BPs) and metabolic disturbances during AP.

■ MATERIALS AND METHODS

Animal Experiments. All animal experimental procedures were approved by the Animal Ethics Committee of West China Hospital, Sichuan University (20211706A). 6−8 weeks old male C57BL/6J mice were purchased from Beijing Huafukang Bioscience Co., Ltd. (Beijing, China) and housed, up to five per cage, in a specific pathogen-free experimental animal center of West China Medical School on a 12 h light/12 h dark cycle at 25 °C. Mice weighing 20−22 g were randomly grouped after 1 week of adaptive feeding. Food and water were supplied ad libitum. The AP model groups were established by injection of CER (50 μg/kg body weight, i.p.) at an hourly interval and sacrificed at the corresponding time point (4, 7, 12, and 24 h) from the first injection of CER (0 h). Mice from the control group (Con) were treated with seven injections of phosphate-buffered saline at 1 h interval. The pancreas was removed and immediately snap frozen in liquid nitrogen and then stored at −80 °C until further processing. Blood samples were subjected to centrifugation at 1500g for 15 min at room temperature, and the supernatant was collected and stored at −80 °C until processing.

Histopathology, Biochemical Index Assessment, and Statistical Rationale. Pancreatic tissue was fixed in 10% formalin, embedded in paraffin, sectioned into 2 μm, and used for hematoxylin and eosin (HE) staining. The pancreas histological damage scoring, serum amylase, and lipase were measured according to our previous study.[17] HE and biochemical index were analyzed from seven mice per group. Statistical power was deemed to be sufficient based on our previous observations in the CER-AP mice model.[17] All the statistical analyses were performed using GraphPad Prism 8.3.0. The results of biological data were presented in mean ± SEM and tested for normality and variance. A Student's t-test was used to compare two groups, or one-way ANOVA analysis followed by Bonferroni post hoc test to compare multiple groups. A probability level of 0.05 was used as the threshold of significance.

Mass Spectrometry Sample Preparation and Measurement. *Proteins.* Pancreas samples from mice were prepared for mass spectrometry. Briefly, approximately 20 mg of the pancreas (n = 4 per group) was homogenized in 600 μL of T-PER tissue protein extraction reagent (Thermo Fisher Scientific, 78510) containing protease inhibitor and vortex at 4 °C for 30 min to disrupt the tissue, repeated twice. Cell debris and insoluble substances were removed by centrifugation at 15,000g for 20 min. The supernatant was collected and quantitated by the bicinchoninic acid (BCA) assay. Extracted proteins (200 μg) from each sample were supplemented to 200 μL in 50 mM ammonium bicarbonate and precipitated by 1 mL of pre-cooled acetone overnight at −20 °C. After centrifugation, the supernatant was removed, and the samples were dried at a fume hood. The precipitation was redissolved and reduced by dithiothreitol in 8 M urea buffer to a final concentration of 10 mM at 37 °C for 3 h. Then, samples were alkylated to block the free cysteine residues by adding 1 M iodoacetamide to a final concentration of 25 mM and incubated in darkness for additional 30 min. The buffer of alkylated protein was exchanged from 8 M urea to 50 mM ammonium bicarbonate by 10 kDa ultrafiltration centrifugal device (PALL, OD010C34). The protein was digested by adding 4 μg of sequence grade trypsin (Promega, V5117), which was dissolved in 50 mM ammonium bicarbonate at 37 °C and kept for 16 h. The solution containing peptides were then centrifuged at 10,000g for 15 min and washed with 50 μL of ammonium bicarbonate twice. All eluted peptide solutions were pooled and added with 20% trifluoroacetic acid to a final 0.4% v/v concentration. The concentration of each peptide solution was determined by the Pierce quantitative colorimetric peptide assay kit (Thermo Fisher Scientific, 23275). A part of the peptides from each sample were combined and used for fraction, which was performed on a reversed phase high-performance liquid chromatography (Vanquish, Thermo Fisher Scientific) under basic pH, with a mobile phase consisting of buffer A (98% water with 2% acetonitrile, pH = 10) and buffer B (98% acetonitrile with 2% water, pH = 10). A standard 43 min LC gradient run was used as below: 0−5 min, 2−2% buffer B; 5−7 min, 2−5% buffer B; 7−27 min, 5−18% buffer B; 27−37 min, 18−32% buffer B; 37−38 min, 32−90% buffer B; 38−40 min, 90% buffer B; 40−41 min, 90−2% buffer B; 41−43 min, 2% buffer B, and the flow rate was 1 mL/min. The peptide mixture was separated into 39 fractions and combined into 13 fractions. All peptides were desalted and dried in the speed vacuum (Christ).

LC−MS/MS Analysis. The desalted peptides were resuspended in buffer A (0.1% formic acid). Equal quantity of iRT peptides (Biognosys, ki-3002-1) was added to each peptide sample to correct the retention time (RT) of peptides. All peptide samples were separated on a homemade capillary column (75 μm i.d. × 25 cm, ReproSil-Pur C18-AQ, 1.9 μm; Dr. Maisch) and measured via LC−MS/MS using an EASY-nLC 1200 system coupled to an Orbitrap Exploris 480 mass spectrometer (Thermo Fisher Scientific). The column temperature was set at 55 °C. The mobile phase was composed of buffer A (0.1% formic acid) and buffer B (80% acetonitrile, 0.1% formic acid), and eluted at 300 nL/min with a gradient as follows: 0−4 min, 3−8% buffer B; 4−71 min, 8−28% buffer B; 71−81 min, 28−40% buffer B; 81−83 min, 40−95% buffer B; and 83−90 min, 95% buffer B. In MS, DIA is a method of molecular structure determination in which all ions with a selected m/z range are fragmented and analyzed in a second stage of tandem MS, tandem mass spectra are recorded either by fragmenting all ions that enter the mass spectrometer at a given time or by sequentially isolating and fragmenting ranges of m/z, while DDA is a method of molecular structure determination where a fixed number of precursor ions are selected and analyzed by tandem MS.[35−37] The fractionated peptides used for establishing library were analyzed on LC−MS/MS using data-dependent acquisition (DDA). The mass spectrometer was acquired in the positive ion mode with a capillary temperature of 320 °C and a spray voltage of 2300 V. Mass spectra were recorded in the Orbitrap analyzer with a mass range of 350 to 1200 m/z, a resolution of 60,000 with the automatic gain control (AGC) target of 300%, and at a maximum injection time of 50 ms. Higher-energy C-trap dissociation peptide fragments acquired at 30% normalized collision energy (NCE) were analyzed at a resolution of 15,000 in the Orbitrap analyzer with an AGC target of 75%, and at a maximum inject time of 22 ms with isolation window set at 1.6 m/z. Dynamic exclusion was set at 30 s, mass tolerance of ±10 ppm was allowed, and the precursor intensity threshold was set at 2×10^4. All the other peptide samples were acquired using the data independent acquisition (DIA) method. The full scan was performed between 350 and 1200 m/z with 60,000 resolution. The AGC target was set to 300% and maximum injection time was 50 ms. Then, 60 DIA windows (Table S1) scanned from 350 to 1200 m/z with a resolution of 15,000 where precursor ions were fragmented with NCE set at 33% and analyzed with AGC target of 200% and auto maximum injection time.

Lipids. Approximately 10 mg of each pancreatic tissue sample collected from AP and control groups (*n* = 7 per group) were homogenized in 940 μL of water at 4 °C using TissueLyser [Jieling Instrument Manufacturing (Tianjin) Co., LTD]. All homogenate was added to 2 mL of methanol and 0.9 mL of dichloromethane for extraction, and the mixture was vortexed. Then, 3 μL of SPLASH LipidoMIX internal standard (Avanti Polar Lipids) was added to the mixture, shook, and incubated for 30 min at room temperature, followed by adding another 1 mL of water and 0.9 mL of dichloromethane, shaking again. The lower organic phase enriched in lipids was collected after centrifuging at 2000 rpm for 10 min, and the upper phase was reextracted by 2 mL of dichloromethane. The twice extracted organic phase was dried in a nitrogen blow-dryer (Biotage). The dried sample was reconstituted in 100 μL of methanol and dichloromethane (1:1, v/v) for lipidomic analysis.

LC−MS/MS Analysis. The targeted lipidomics analysis were analyzed by LC−MS/MS using a SCIEX Triple Quad 5500+ mass spectrometer equipped with a LC-20AD UPLC system (Shimadzu) on an HSS T3 column (1.8 μm, 2.1 mm × 100 mm, Waters) at 55 °C, controlled by Analyst 1.7.2 software (SCIEX). The chromatographic method was performed according to a previous study.[38] The mobile phases buffer A was composed of acetonitrile and water (40:60, v/v) with 10 mM ammonium acetate, whereas the mobile phase buffer B consisted acetonitrile and isopropanol (10:90, v/v) with 10 mM ammonium acetate. The gradient was performed as follows: 0−10 min, 40 to 100% buffer B; 10−12 min, 100% buffer B, 12−12.1 min, 100 to 40% buffer B, 12.1−15 min, 40% buffer B. The flow rate was set to 0.5 mL/min and the sample injection volume was 1 μL. Data were acquired in positive mode with 867 scheduled multiple reaction monitoring (MRM) transitions and negative mode with 1267 scheduled MRM transitions, respectively (Table S2). Electrospray ionization source parameters were set as follows: ion GS1 set at 50 psi, GS2 set at 60 psi, curtain gas set at 35 psi, temperature of 400 °C, and spray voltage of 5.2 kV in positive mode as well as the temperature of 450 °C and spray voltage in the negative mode.

Mass Spectrometry Data Analyses. *Pancreatic Proteome.* The DDA data raw files for fractionated peptides were analyzed using Spectronaut 15.4.210913.50606 (Biognosys), and MS/MS spectra were searched against the UniProt mouse proteome database (17033 entries, 2020/04/26) and the Biognosys iRT peptide sequences (11 entries) to generate the spectral library for this study. The default settings were used unless otherwise described. The false discovery rate (FDR) was set to 0.01 for peptide and protein identifications. An in-house spectral library of mouse pancreas was generated, which contained 80,134 precursors, 66,894 peptides, 7954 proteins, and 7848 protein groups, and it also included mass spectrometric and chromatographic parameters such as the precursor and fragment m/z, relative intensity of fragment ions, and RT for each peptide precursor.[37,39] The DIA raw data for pancreatic samples were processed using Spectronaut against the in-house library with the default settings. The optimal extraction window was dynamically determined by the Spectronaut based on gradient stability and iRT calibration. The RT was predicted based on dynamic iRT. The mass tolerance for both MS1 and MS2 was set to dynamic. Identifications for peptides and proteins were filtered with a *q*-value cutoff of 0.01, and MS2 spectra were used for relative quantification.

Pancreatic Lipidome. The MRM raw data were processed using SCIEX OS-Q 2.1.6 (SCIEX), the integration parameters were set as default settings, and the inaccurate peaks were corrected by hands-on manual intervention.

Bioinformatic Analyses. Bioinformatics analyses in raw data of protein intensities and lipid intensities were performed using the Wukong platform (http://www.omicsolution.org/wu-kong-beta-linux/main/), unless otherwise stated. Protein data were imputed to fill missing values (<50%) using the k-nearest neighbor (KNN) algorithm and further normalized by the median. Significantly changed proteins over multi-time points were screened by time-course analysis, with Hotelling T^2 (HT^2) = 18 as a cutoff value. These proteins were further clustered by hierarchical clustering analysis (HCA) using Z-score normalized data and shown in the heatmap. Furthermore, they were supplied in Gene Ontology (GO) annotation,
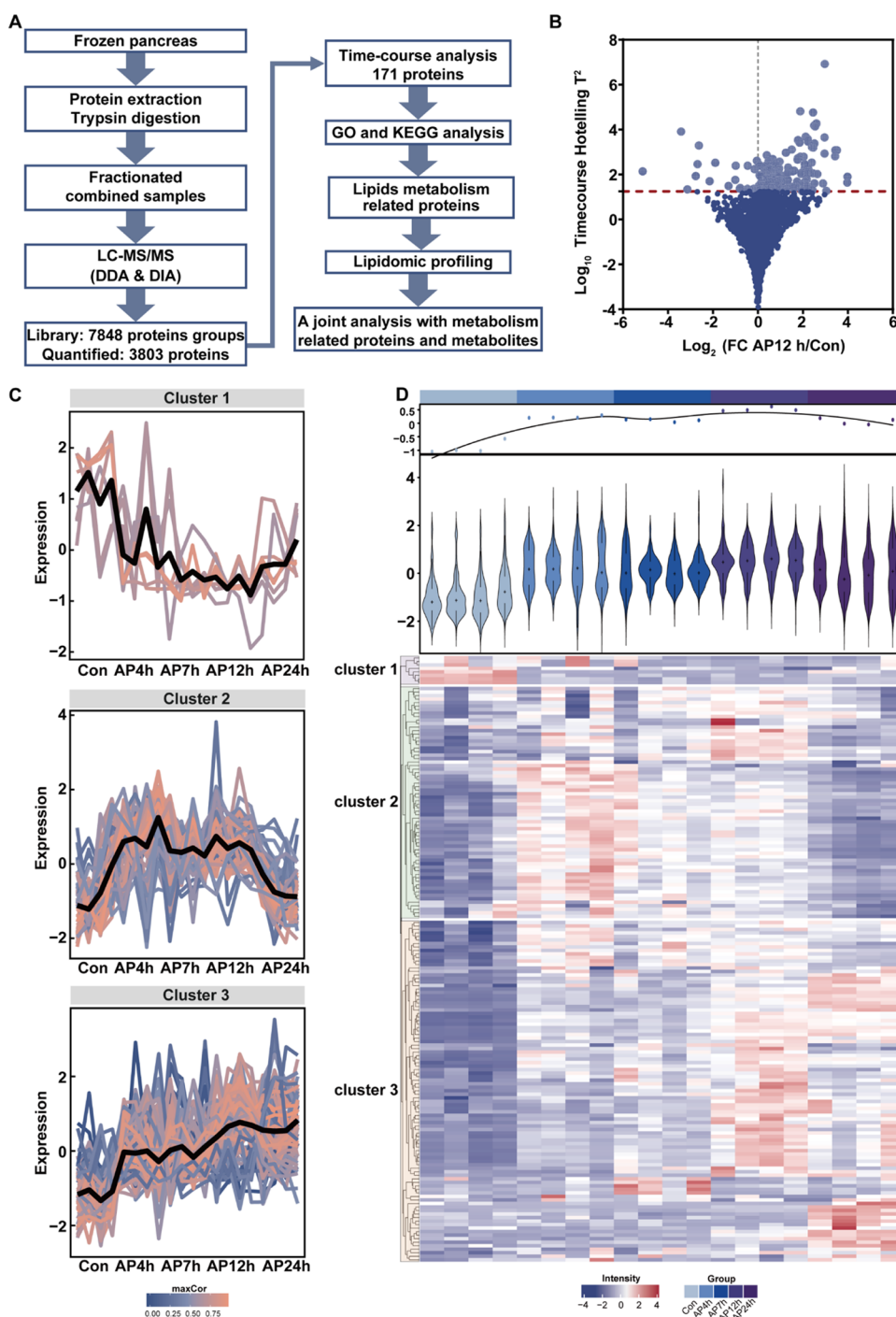
Figure 1. Temporal profiles for significant changed proteins in CER-AP mice model. (A). The schematic illustration for integrated proteomics and lipidomics analysis. (B) The volcano plot displayed the significant changed proteins along all time points by a time-course analysis with the Hotelling T^2 value on Y-axis and fold change (FC) value (AP12h/Con) on X-axis. (C) Hierarchical cluster analysis of 171 changed proteins over 24 h into three clusters and (D) their expressions were normalized and presented in heatmap combined violin plots. The color bar from blue to red represents each sample intensity after normalization using the Z-score.

Kyoto Encyclopedia of Genes and Genomes (KEGG) enrichment analysis, and UniProt keyword terms. The polar plot, variant chord plot, upset plot, network plot, terms network plot, and ridgeline were visualized in EnrichVisBox (https://www.omicsolution.com/wukong/EnrichVisBox/). The top 10 GO terms supplied in BP, cellular component (CC), and molecular function (MF) were separately ranked by FDR < 0.05 and counts/annotate ratio. The top 20 terms displayed in KEGG pathway analysis were ranked by counts.

The intensity of changed proteins across each time point were compared by ANOVA followed by post hoc test FDR, and the bar plots were visualized in GraphPad Prism 8.3.0. The protein−protein interaction (PPI) networks were analyzed by STRING (https://string-db.org/) and visualized in Cytoscape 3.6.0. The resulting raw data of lipid measurements were preprocessed by corresponding IS, QC, and total strength in both positive and negative modes. The normalized data were combined and categorized into various lipid classes shown in
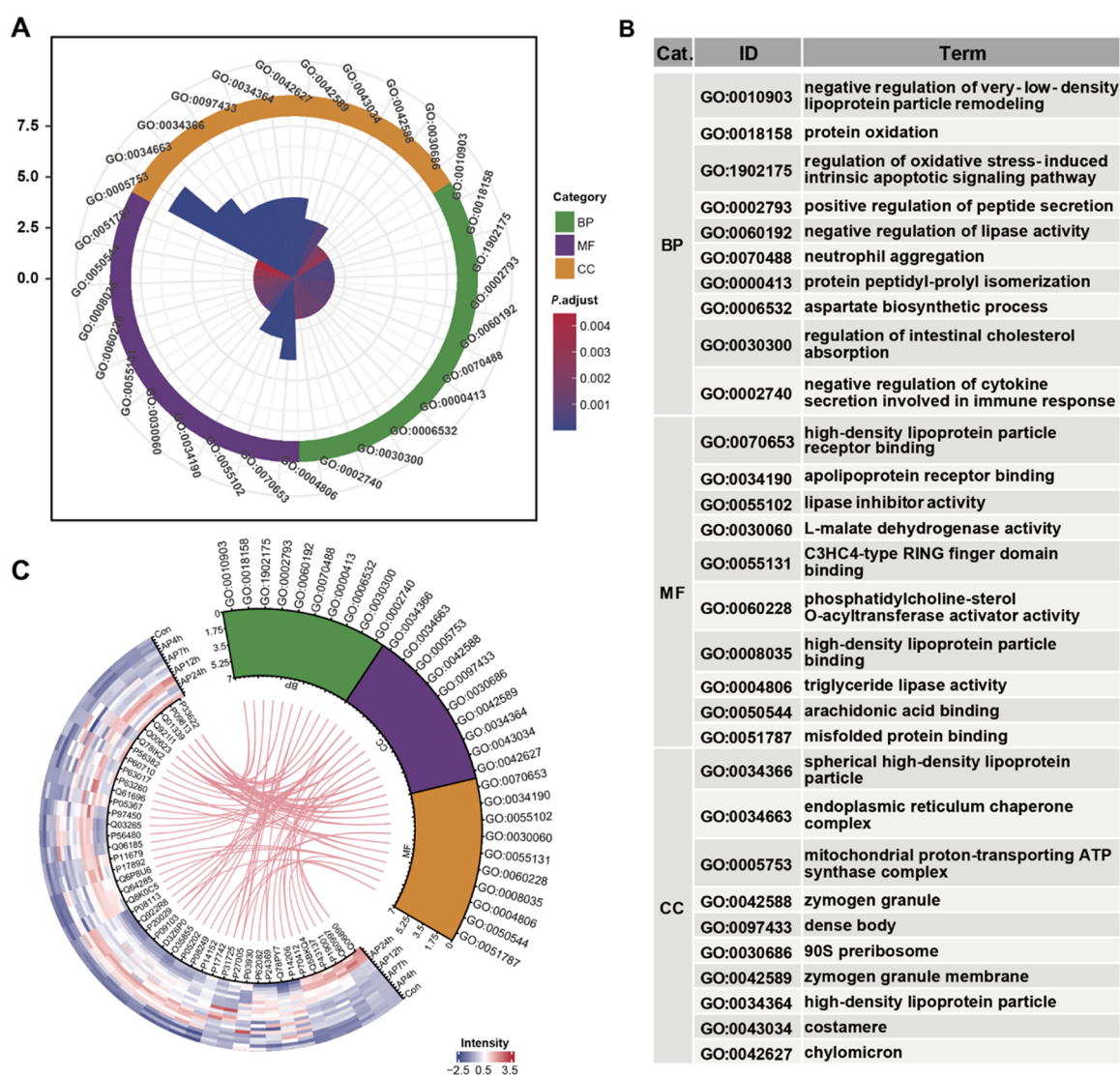
Figure 2. Pancreatic changed proteome displayed enriched lipids related regulation and metabolism process by GO analysis. (A) The polar plot showed the top 10 terms in BP (in green), CC (in purple) and MF (in orange) sub-ontologies. (B) The detailed description and GO ID for each term was provided. (C) The variant chord plot showing the link between protein abundance (44 projects) and GO-enriched terms (top 10). The outer circle indicated the top 10 terms in BP, CC, and MF (on the right) and 44 proteins with their abundance in different time points (on the left). The color bar from blue to red represents each sample intensity after normalization using the Z-score. The undirected pink edges inside the circle displayed the interactions of a particular protein with their respective connected GO terms.

the scatter diagram. A Mfuzz analysis was used to divide the temporal lipids intensities into six clusters and proportions of each lipid subclasses were accordingly calculated. Simultaneously, significantly changed lipids over multi-time points were screened by time-course analysis with Hotelling $T^2 = 30$ as a cutoff value. The temporal trajectory for these changed lipids were analyzed in principle components analysis (PCA) by MetaboAnalyst 5.0. The changed lipids were normalized by the Z-score and displayed in the heatmap, and in particular, the lipid species with the highest HT^2 value were shown in the line chart by GraphPad Prism 8.3.0. Lastly, the targeted aqueous metabolomics data used in the joint analysis were obtained from our previous study,[17] and the preprocess method was the same as before.

■ RESULTS

Temporal Profiles of Important Proteins Altered in the CER-AP Mice Model. Pancreatic protein samples from

Con, 4, 7, 12, and 24 h AP mice were analyzed using LC−MS/MS. According to the HE exam and biochemical index (Figure S1), an inflammatory peak was seen at 12 h, which was in line with our earlier findings.[17] We obtained the relative quantitative data for a total of 3803 proteins in comparison to the in-house library (Figure 1A). Good reproducibility between biological replicates was apparent (Pearson's r range: 0.9679−0.9993), which was higher than between samples from different phenotypes (Pearson's r range: 0.5958−0.9960). A number of proteins with various upregulated and down-regulated patterns were chosen based on time-course analysis with the Hotelling T^2 statistic bigger than 18 since we were interested in how proteins altered over time (Figure 1B and Table S3). There were found to be 171 proteins in all, divided into three clusters. The metabolic enzymes hydroxymethylglu-taryl-CoA synthase (Hmgcs2), protease inhibitors serine protease inhibitor EIC (Serpin b1c), and serine protease inhibitor EIA (Serpin b1a), fatty acid-binding protein,
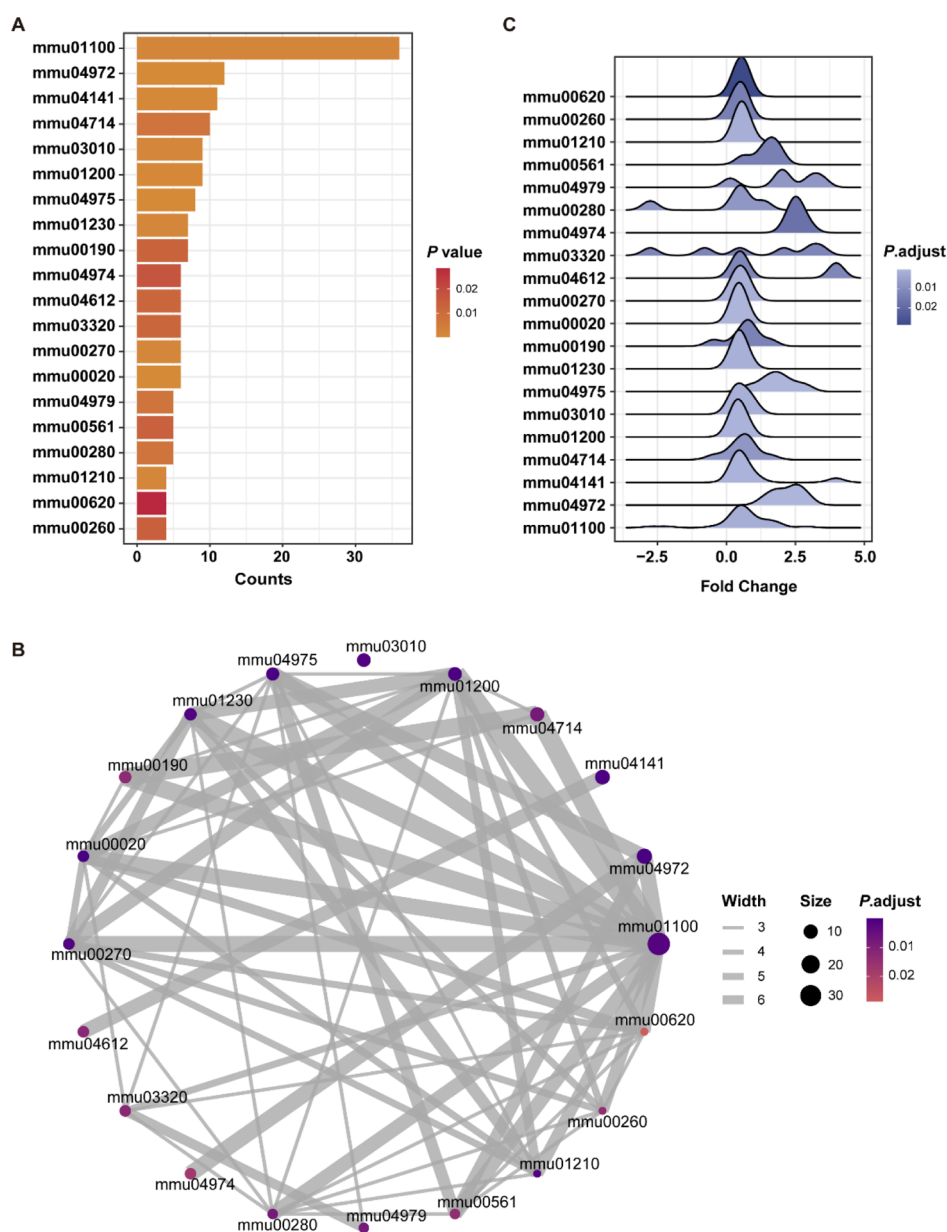
Figure 3. AP dysregulated metabolic pathways with pancreas. (A) KEGG pathway analysis on the 171 changed proteins. The IDs on the vertical axis correspond to the top 20 KEGG pathways. mmu01100, metabolic pathways; mmu04972, pancreatic secretion; mmu04141, protein processing in ER; mmu04714, thermogenesis; mmu03010, ribosome; mmu01200, carbon metabolism; mmu04975, fat digestion and absorption; mmu01230, biosynthesis of amino acids; mmu00190, oxidative phosphorylation; mmu04974, protein digestion and absorption; mmu04612, antigen processing and presentation; mmu03320, PPAR signaling pathway; mmu00270, cysteine and methionine metabolism; mmu00020, citrate cycle (TCA cycle); mmu04979, cholesterol metabolism; mmu00561, glycerolipid metabolism; mmu00280, valine, leucine, and isoleucine degradation; mmu01210, 2-oxocarboxylic acid metabolism; mmu00620, pyruvate metabolism; and mmu00260, glycine, serine, and threonine metabolism. (B) A network plot with edges displaying overlapped proteins among the enriched 20 pathways. The line size of the edges corresponds to the number of overlapped proteins between two terms. (C) The ridgeline exhibited the density distribution of all proteins FC (AP 12 h/Con) across each KEGG ID.

adipocyte (Fabp4), as well as other proteins involved in cell growth and survival, were assigned in cluster 1 (Table S4), which contained eight proteins and displayed a major decrease expression over 24 h (Figure 1C). Additionally, 66 proteins belonged to cluster 2 with an increasing peak at 4 to 12 h primarily including metabolic enzymes branched-chain amino acid aminotransferase, mitochondrial (Bcat2), aspartate aminotransferase, mitochondrial (Got2), malate dehydrogenase, cytoplasmic (Mdh1), malate dehydrogenase, mitochondrial (Mdh2), isocitrate dehydrogenase, mitochondrial (Idh2), aconitate hydratase, mitochondrial (Aco2), and succinate dehydrogenase (Sdhd), D-3-phosphoglycerate dehydrogenase (Phgdh), and phosphoserine aminotransferase (Psat), as well as several ATP synthases (Table S4). Evidently, the majority of proteins were concentrated in the third cluster and showed a general upward tendency over time (Figure 1C). There were 97 proteins in all, most of which were common hydrolase such as pancreatic alpha-amylase (Amy2), anionic trypsin-2 (Prss2), chymotrypsin-like elastase family member 1, 2A, and 3b (Cela1, Cele2a, and Cela3b), carboxylesterase 1C (Ces1c), carboxypeptidase A1 and A2 (Cpa1 and Cpa2), phospholipase A2 (Pla2), and colipase (Clps); response stress proteins heat
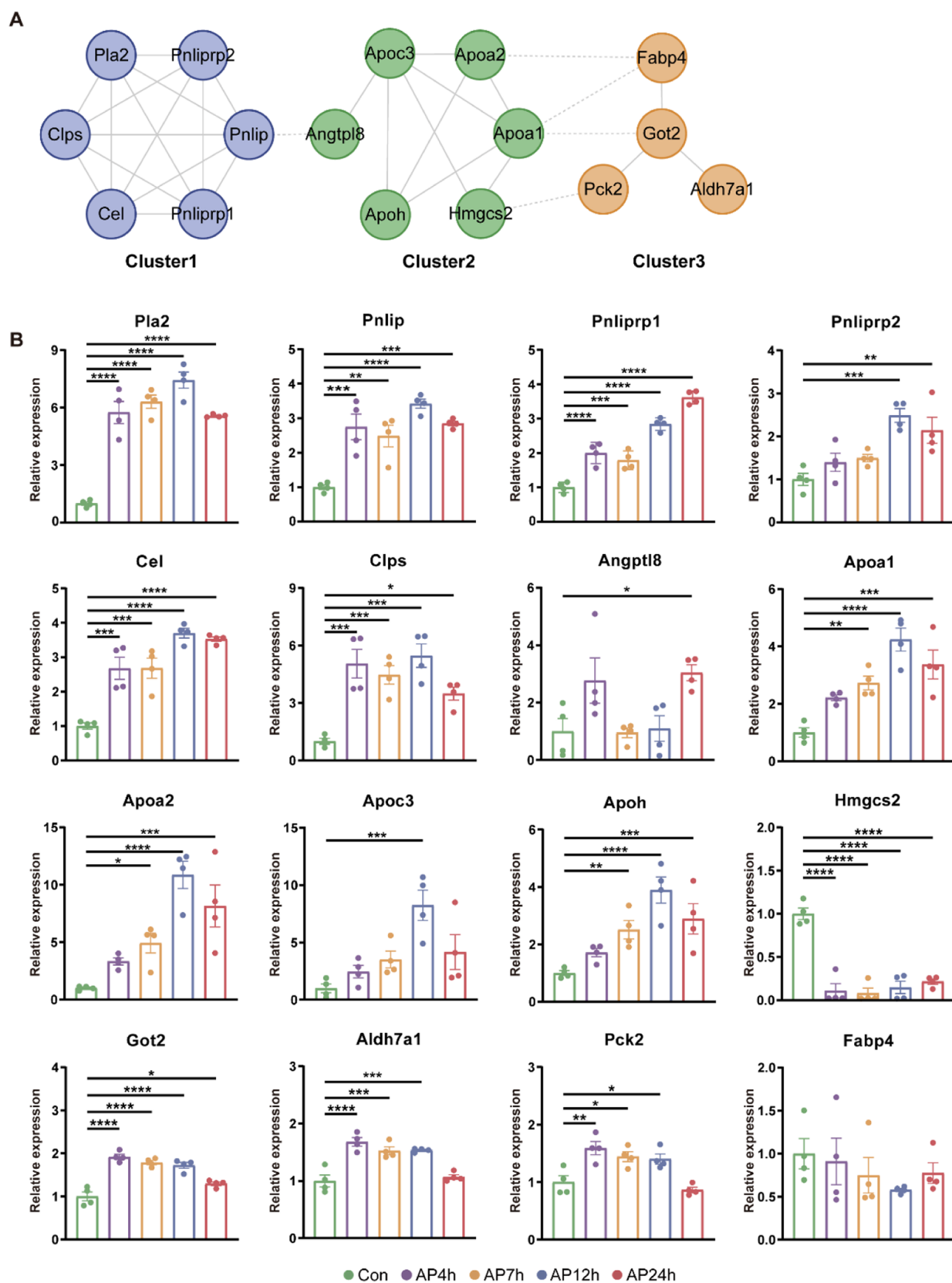
Figure 4. Differentially expressed proteins involved in lipid metabolism and their interactions during the AP course. (A) String analysis of the PPI network for 16 proteins attributed to lipids metabolism which were mainly divided into three clusters by k-means clustering. (B) Relative expressions of 16 changed proteins. Errors bars represent standard error of the mean (SEM). *$P < 0.05$, **$P < 0.01$, ***$P < 0.001$, and ****$P < 0.0001$ vs Con.

shock 70 kDa protein 1A, 2, and 8 (Hspa1a, Hsp2, and Hspa8), and heat shock 25 kDa protein (Hsp 25); metabolic enzymes aldehyde oxidase 3 (Aox3); as well as serine protease inhibitor A1a, A1b, A1e, A3K, A3N, and kazal-type 1 (Serpina1a, Serpina1b, Serpina1e, Serpina3k, Serpina3n, and Spink1) (Table S4). Figure 1D shows the scaled data for the 171 protein expressions as a heatmap and the total changes as violin plots.

The Pancreatic Proteome Displayed Enriched Lipids Related Regulation and Metabolism Process. These 171 proteins were annotated using the GO classification to better investigate their functions. In detail, a total of 1299 entries were enriched, consisting of 837 GOBP terms, 195 GOCC terms, and 267 GOMF terms (Table S5). Figure 2A,B shows the top 10 terms in each sub-ontology in rank by FDR and count ratio. The abundance of 44 proteins at serial-time points annotated to the top 10 root category terms is displayed as a variant chord plot in Figure 2C. To be more specific, 18 proteins from cluster 2 and 26 proteins from cluster 3 (Figure 1C) were enriched in these top GOBP, GOCC, and GOMF terms (Table S6). Among them, metabolic enzymes Bcat2, Got2, Mdh1, and Mdh2 were principally enriched into GO terms GO: 0006532 (aspartate biosynthetic process) and GO: 0030060 (L-malate dehydrogenase activity). Additionally, the majority of the terms in GOBP and GOMF are primarily related to lipids metabolism regulation, such as the terms for negative regulation of very-low-density lipoprotein particle remodeling (GO: 0010903), negative regulation of lipase activity (GO: 0060192), regulation of intestinal cholesterol absorption (GO: 0030300), high-density lipoprotein particle receptor binding (GO: 0070653), apolipoprotein receptor binding (GO: 0034190), lipase inhibitor activity (GO: 0055102), high-density lipoprotein particle binding (GO: 0008035), and triglyceride lipase activity (GO: 0004806). The overlap between each pair of terms is then shown in Figure S2. Out of 44 proteins, apolipoprotein A-I (Apoa1) and Apoa2 were each implicated in up to 13 GO terms.

AP Dysregulated Metabolic Pathways with Pancreas. KEGG pathway analysis of 171 changed proteins showed 174 enriched pathways, of which 26 pathways had an adjusted p value of less than 0.05. These 26 pathways were mostly categorized into metabolic pathways (14/26), pancreatic secretion, fat digestion, and absorption, as well as protein processing in ER (Table S7). It was suggested that pancreatic enzyme secretion, protein processing, and metabolic dysregulation are vital mechanisms during the early stage of AP based on the edematous animal model. Ranked by counts, the top 20 related pathways are shown in Figure 3A, metabolic pathways (mmu01100) with 36 counts ranked first, pancreatic secretion (mmu04972) with 12 counts, and protein processing in ER (mmu04141) with 11 counts also occupied the front positions. To further identify the overlapped objects, an interaction network between two enriched terms was built. In a nutshell, pancreatic secretion (mmu04972) interacted with protein digestion and absorption (mmu04974), glycerolipid metabolism (mmu00561), as well as fat digestion and absorption (mmu04975), while terms connected to metabolism almost interacted with thermogenesis (mmu04714). Additionally, antigen processing and presentation (mmu04612) intersected with protein processing in the ER (mmu04141). Ribosome (mmu03010) was distinct and did not correlate with any other terms (Figure 3B). Parallel to this, the majority of protein abundance variation displayed a normal distribution in each

term (Figure 3C), and Figure S3 indicated the specific assignments between terms and protein objects.

Functions of Differentially Expressed Proteins Involved in Lipid Metabolism during AP. Sixteen proteins involved in four lipid metabolism and signaling pathways (mmu04795, mmu03320, mmu4979, and mmu00561) were further identified and annotated (Table S8) in order to link the results of the KEGG enrichment analysis to the observed altered lipids metabolism process. These proteins' PPI network string analysis revealed that k-means clustering primarily separated them into three groupings (Figure 4A). Six proteins from cluster 1 were involved in the catabolic process of triacylglycerols (TAGs), six proteins from cluster 2 were involved in lipid transport and cholesterol metabolism, and four proteins from cluster 3 were involved in lipid metabolism. Except for HMGCS2 from cluster 2, which catalyzes the first irreversible step in ketogenesis, condensing acetyl-CoA to acetoacetyl-CoA to generate HMG-CoA was essential for cholesterol, steroid, and lipid biosynthesis, most proteins showed increasing trends from 4 to 24 h (Figure 4B). This finding suggested that at the onset of AP, cholesterol and steroid production were reduced. Other pancreatic proteins, including apolipoproteins A-I (Apoa1), A-II (Apoa2), and C-III (Apoc3), also peaked at 12 h and subsequently started to decline. Apoa1 is the primary protein in HDL, which is crucial for maintaining healthy levels of cholesterol by carrying additional cholesterol from extrahepatic tissues to the liver.[40] In patients with predicted severe AP, lower serum levels of Apoa1 were linked to a more pronounced inflammatory state and were used as a measure to predict persistent organ failure.[41] Therefore, it is important to pay more attention to the uneven pattern of protein changes in the serum and pancreas. Additionally, triglyceride hydrolysis was thought to be the cause of an increase in proteins from cluster 1. For instance, pancreatic triacylglycerol lipase (Pnlip) split long-chain fatty acid esters at positions 1 and 3 to produce primarily 2-monoacylglycerol and free fatty acids (FFAs) from triglycerides, which was a significant contribution to this process. It was hypothesized that Pnliprp1 would facilitate calcium ion binding and the breakdown of triglycerides. Pnliprp2 predominantly hydrolyzes medium- and long-chain fatty acyls in galactolipids and short-, medium-, and long-chain fatty acyls in triglycerides without apparent positional selectivity. A hormone regulator, angiopoietin-like protein 8 (Angptl8) regulates blood triglyceride levels. Likewise, the number of proteins that hydrolyze phospholipids rose. For instance, Pla2 hydrolyzed the ester bond of the fatty acyl group linked to the phospholipid's sn-2 position, preferring phosphatidylethanolamines (PEs) and phosphatidylglycerols (PGs), while bile acids-activated lipase (Cel) catalyzed the hydrolysis of a variety of substrates, such as cholesteryl esters (CEs), phospholipids, lysophospholipids, di- and tri-acylglycerols, and fatty acid esters of hydroxy fatty acids. Cluster 3 mainly includes metabolic enzymes phosphoenolpyruvate carboxykinase (Pck2), Got 2, aldehyde dehydrogenase family 7, member A1 (Aldh7a1), and fatty acid transport protein. Aldh7a1 can protect cells from oxidative stress by metabolizing a number of lipid peroxidation-derived aldehydes. Together, alterations in the abundance of proteins involved in hydrolase and the transport, absorption, and catabolism of lipids suggested that the metabolism of downstream phosphoglycerides, glycerides, cholesterol, and fatty acids during AP was dysregulated.
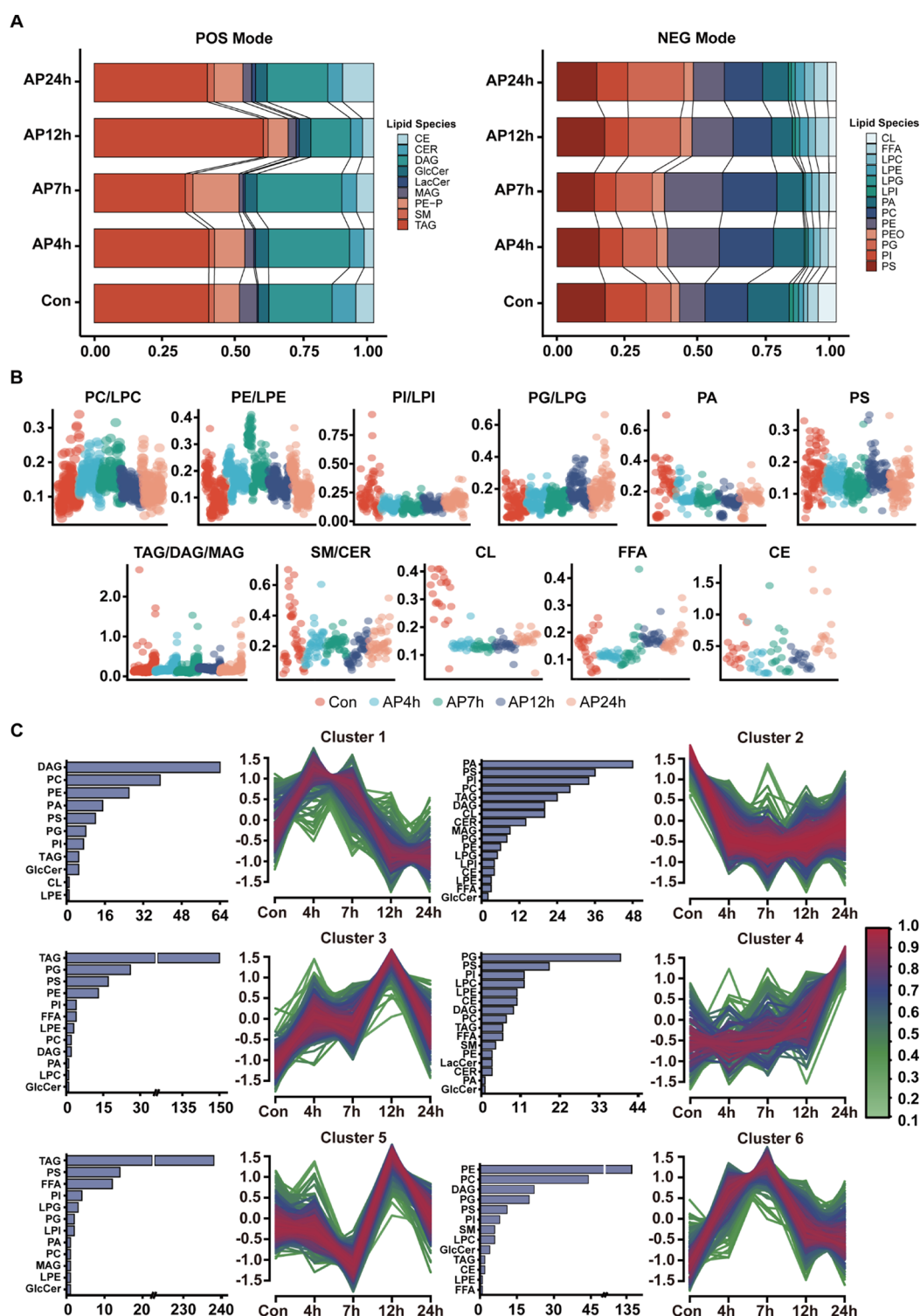
Figure 5. Perturbations of pancreatic lipidome profiling uncovered changing rule for unsaturated fatty acyls. (A) The percentage stacked column charts indicated the proportion of each lipid species in both positive (left) and negative (right) modes. (B) The lipid subclasses were grouped according to their interconverted relationship and presented in the scatter plots for the five time-point groups. (C) Mfuzz clustering analyses divided the 1364 lipids altered in pancreas during the AP progress into six clusters. The number of lipids enriched in each cluster was shown in a bar graph aside.

Pancreatic Lipidome Profiling Changes Revealed a Shifting Rule for Unsaturated Fatty Acyls. The aforementioned dyslipoproteinemia signature suggested a possible lipidome imbalance. One microliter of pancreatic extractions was subjected to a targeted wide-coverage lipidomics analysis in both positive and negative modes, and the results revealed 661 lipids from 9 different lipid subclasses and 703 lipids from 13 various lipid subclasses. The accurate detection was explained by the IS coefficient of variations that were calculated in Table S9. TAGs and phosphatidylcholines (PCs) were the two species that were found to be the most prevalent, as shown in Figure 5A, which also shows that the
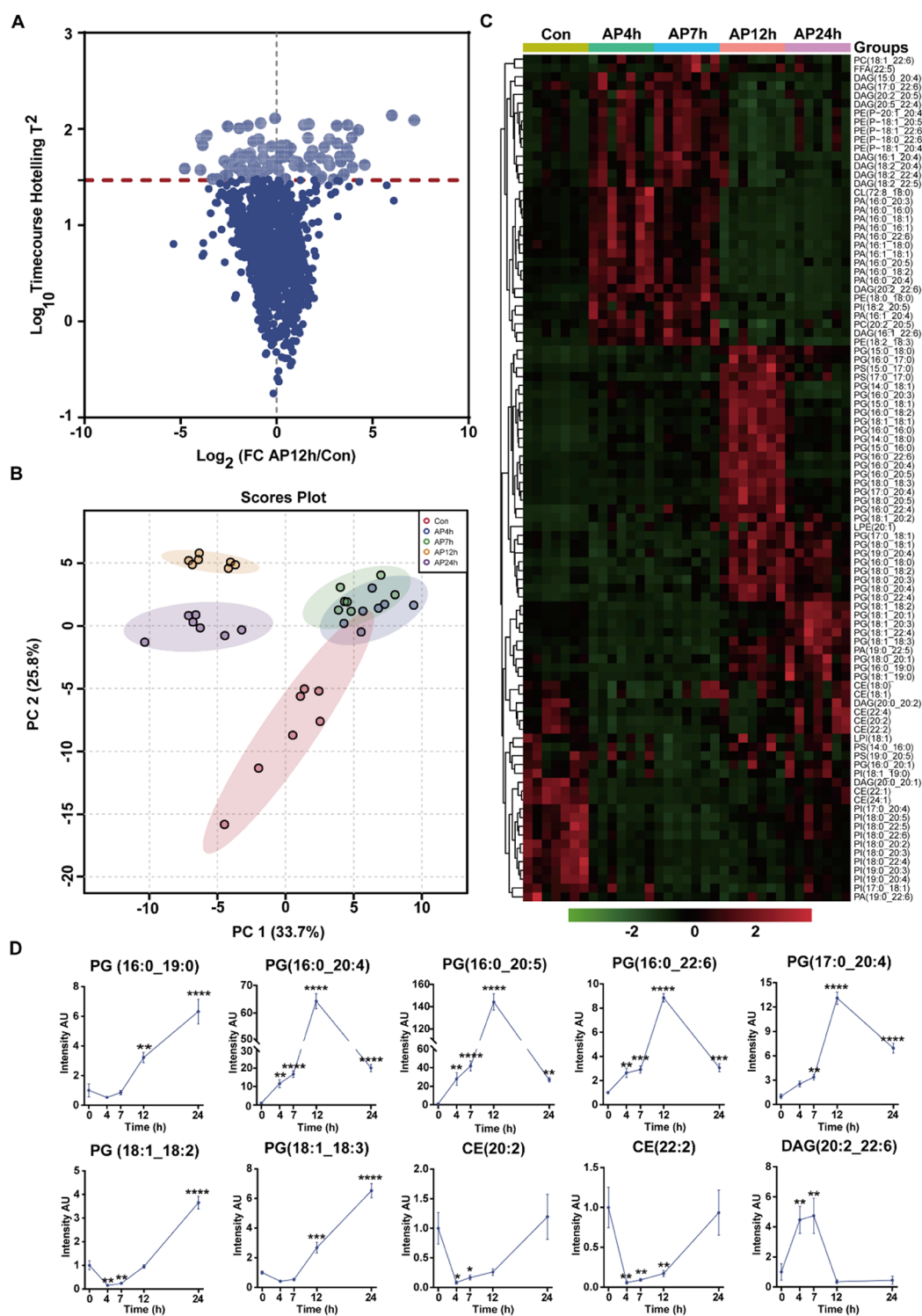
Figure 6. Time-course changes of pancreatic lipids pattern interpreted constant disturbed phosphoglycerides during AP. (A) The volcano plot displayed the significant changed lipids along all time points by a time-course analysis with Hotelling T^2 value on Y-axis and FC value (AP12h/Con) on X-axis. (B) The PCA score plot for con and AP time-point groups analyzed by 96 changed lipid intensities. (C) Heatmaps of 96 changed lipids covering multi-time points. The color bar from green to red represents each sample intensity after normalization using Z-score. (D) The line chart showed the top 10 disturbed lipids with the largest $\mathrm{H}T^2$ value by time-course analysis. Errors bars represent SEM. *$P < 0.05$, **$P < 0.01$, ***$P < 0.001$, and ****$P < 0.0001$ vs Con group.

pancreatic lipidome species abundance corrected by IS and divided by the total ion intensities were obtained as C percent across multiple time points. Sixteen CEs, 17 ceramides (Cers), 14 glucosylceramides (GlcCERs), 3 lactosylceramides (LacCERs), 10 sphingomyelins (SMs), 49 phosphatidyletha-nolamines (PEs-P), 425 TAGs, 117 diacylglycerols (DAGs), and 10 monoacylglycerols (MAGs) were detected in the positive mode, as well as 19 lysophosphatidylcholines (LPCs), 121 PCs, 19 lysophosphatidylethanolamines (LPEs), 110 PEs, 26 ether-containing PEs-O, 8 lysophosphatidylglycerols
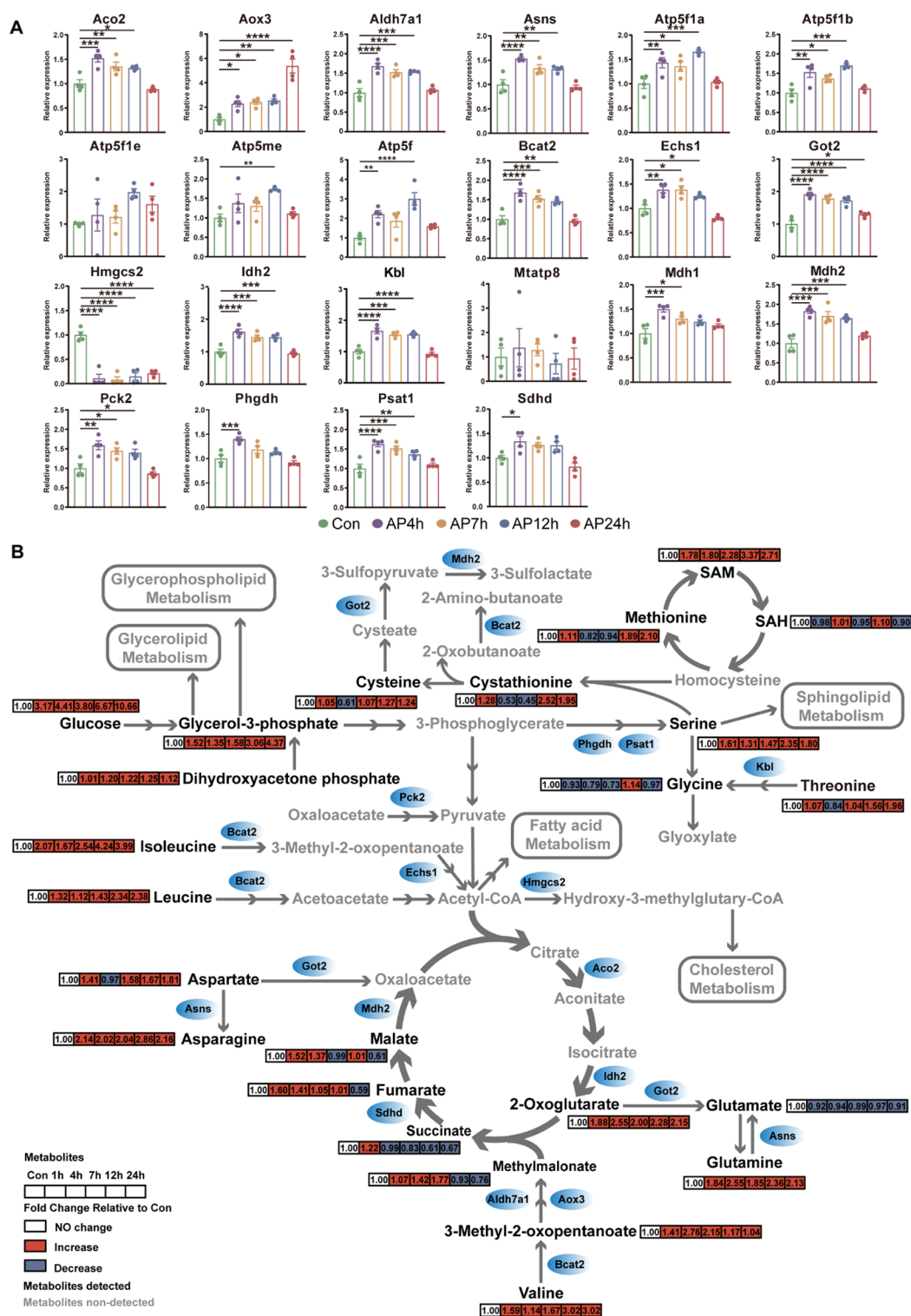
Figure 7. Integrated pancreatic proteomics and metabolomics revealed altered amino acid and central carbon metabolism in CER-AP. (A) Relative expressions of proteins involved in metabolic pathways were displayed. Errors bars represent SEM. *$P < 0.05$, **$P < 0.01$, ***$P < 0.001$, and ****$P < 0.0001$ vs Con group. (B) Metabolic pathways illustrating primary altered amino acid metabolism and central carbon metabolism identified using temporal proteomics and existing temporal metabolomics data. The related metabolite expression was calculated relative to Con group and shown in red (upregulating) or blue (downregulating) in the box.

(LPGs), 103 PGs, 6 lysophosphatidylinositols (LPIs), 69 phosphatidylinositols (PIs), 109 phosphatidylserine (PS), 21 cardiolipins (CLs), 66 phosphatidic acids (PAs), and 26 FFAs were detected in the negative mode (Table S10). The total content of TAG and DAG disturbed most obviously at 12 h,

whereas the total content of PC and PE disturbed most obviously at 7 h. Figure 5A shows the relative contents change of each lipid subclass. Each lipid subclass was reorganized in accordance with its chemical structure and interconversion and then shown as a scatterplot in the mean of all samples at each

time point in order to analyze the overall content variations in the lipid pool (Figure 5B). Notably, the phosphoglycerides PC/LPC and PE/LPE were significantly disturbed from 4 to 12 h and then recovered at 24 h. CL showed a clear decline from 4 to 24 h, and FFA showed an expected increase following the induction of CER. Then, all the lipids were divided into six clusters using a soft Mfuzz clustering method based on how similar their pattern through time was (Figure 5C). Most TAGs were assigned into cluster 3 and cluster 5, where TAGs with fewer unsaturated bonds in cluster 5 showed a declining trend within 7 h after CER injection, whereas TAGs with polyunsaturated fatty acyl chains in cluster 3 displayed a gradual upward in the first 12 h (Table S11). Except for DAGs clustered in cluster 1, which showed a downward trend at later time points, other DAGs reached their peaks at different time points. Most MAGs clustered in cluster 2 showing a downward trend indicated their mobilization during AP pathogenesis. Although phosphoglycerides alterations are complicated, according to changes from 1 to 7 h, phospholipids dispersed in categories 2 and 5 primarily exhibit a downward trend, whereas categories 1, 3, and 6 primarily exhibit an upward direction. Category 4 did not noticeably change, but elevated at 24 h. Furthermore, phosphoglycerides showing a decreasing trend in categories 2 and 5 mainly include PA, PS, PI, and PC with varied saturation degrees and carbon chain lengths. The changes of FFAs can be divided into two categories, among which 15 saturated FFAs and FFAs with saturation lower than 2 gathered in clusters 2 and 5, which generally show a downward trend in the first 7 h. However, 10 polyunsaturated FFAs clustered in clusters 3, 4, and 6 showed general tendency of rising with varied peaking times, which may be related to the decrease of MAG or phospholipids in clusters 2 and 5 (Table S11).

Pancreatic Lipid Pattern Changes over Time Interpreted Constant Disturbed Phosphoglycerides during AP. A deeper understanding of the distinct lipids implicated in the AP course is critically required after acknowledging the overall lipid species shifting pattern. Time-course analysis with a Hotelling T^2 score greater than 30 was used to screen 96 altered lipids (Figure 6A). Based on the 96 lipid intensities, the unsupervised PCA score plots revealed a lipid metabolic trajectory that was similar to our previously published aqueous metabolite metabolic trajectory.[17] The response started at 4 h, became more noticeable at 7 h, was most distinct at 12 h, and regressed at 24 h (Figure 6B). The opening trajectory also showed that, after 24 h, the metabolism of lipids was still not fully restored. To be more precise, the heatmap (Figure 6C) showed the detailed variation of the 96 lipids abundance. A number of phosphoglycerides, such as PG, PI, PE, PS, and PA, were found, and PI with one polyunsaturated fatty acyl chain displayed a downregulated trend, indicating the likelihood of their hydrolysis. This was in line with earlier studies of aberrant inositol levels in AP patients' peripheral blood.[16] One FFA 22:5 was the only FA chosen, and it was considered a persistently unsettled FA. Eicosapentaenoic acid (EPA) and docosahexaenoic acid can both be produced from docosapentaenoic acid (FFA 22:5). As of yet, there have been no reports about its function in AP. Finally, the line charts showing the top 10 disrupted lipids with the highest HT^2 value were produced (Figure 6D). The importance of examining PG variation in determining biological function is supported by the fact that PGs varied most noticeably at 12 h, even up to 100 times equivalent to control.

Integrated Pancreatic Proteomics and Metabolomics Revealed Altered Amino Acid and Central Carbon Metabolism in CER-AP. We further intended to explain the changes in associated metabolites caused by metabolic enzymes incorporated with our previous metabolomics data (17). A total of nine metabolic pathways (FDR < 0.05) out of the 20 enriched pathways in Figure 3A were found in the pancreas. This investigation shows that the metabolism of carbon, oxidative phosphorylation, TCA cycle, 2-oxocarboxylic acid, cysteine and methionine, glycine, serine, and threonine metabolism, as well as the degradation of valine, leucine, and isoleucine are all greatly affected. Twenty-two proteins were involved in these pathways and they were annotated in Table S12, and their abundance dynamic changes are shown in Figure 7A. As explained in our previous study,[17] dysregulated amino acids metabolism especially cysteine and methionine metabolism were determined. Based on this pancreatic proteomics result, the majority of metabolic enzymes showed a concordant upregulated and returned tendency to satisfy the energy metabolism requirement in AP 4−12 h. This adjustment allowed most of the TCA cycle metabolites, branched chain amino acids (BCAAs), and glycolysis metabolites expressed upregulation in the pancreas during AP (Figure 7B). Nevertheless, several metabolites and metabolic enzymes displayed inconsistent downregulation. For example, the diminished Hmgcs2 together with increased CEs content mirrored insufficient steroid synthesis and excess steroid consumption. Conversely, Aox3, an oxidoreductase with broad substrate specificity, elevated significantly at AP 24 h, indicating that many aldehydes, including valine catabolite methylmalonate semialdehyde, were oxidized to acid (Figure 7B). Related to our previously described cysteine and methionine metabolism, other appropriately varied Bcat2, Got2, Mdh1, and Mdh2 intensities were linked to enhanced catabolism of cysteine.[17] Elevated Phgdh and Psat1 levels also showed increased serine synthesis, which can be utilized for cystathionine synthesis and sphingolipid metabolism.

■ DISCUSSION

The discovery of biological mechanisms and drug targets in AP is facing a huge challenge.[2] AP causes a disrupted pancreatic metabolism and even a systemic metabolic disorder, reflecting the possibility of exploring metabolic mechanisms and targets.[42−44] Here, we integrated temporal proteomics and lipidomics in CER-induced AP mice. Our proteomics investigation places a focus on the proteins that are visibly altered between 0- and 24 h following CER induction. These dysregulated proteins mainly included digestive enzymes, apolipoproteins, lipids metabolism and energy metabolic enzymes, cytoskeletal proteins, heat shock proteins (HSPs), and serine protease inhibitors (SPIs). Furthermore, we focused on 16 proteins relevant to lipid metabolism and regulation function as well as the network of their interactions. Synchronously, lipidomic analysis was conducted to corroborate imbalanced glycerides, phosphoglycerides, sphingolipids, cholesterol esters, and FA profiling to capture the changing rules of unsaturated fatty acyls in them. Finally, as a supplement, based on metabolic enzyme alterations in this study and metabolic data from our prior metabolomics data, we created a comprehensive metabolic profile and indicated the enhanced TCA and amino acid metabolism in CER-AP. As a result, our integrated studies offer a multi-omics approach for AP research using proteomics-led, top-down system biology

methodologies, as well as metabolic insight into the abnormalities associated with AP.

Despite a few to dozens of differentiated proteins in cells or animal models were revealed over the past decade due to easily degradable pancreas, immature two-dimension separation, and MS acquisition method, the new developed high-throughput DIA and DDA strategies, as well as isobaric tagging technology led to the identification of hundreds of changed proteins.[25,26,31,45−48] The development and use of proteomics in AP are strongly tied to the study of numerous molecular mechanisms and the use of digestive enzymes generated by the pancreas as biomarkers of pancreatic illness.[26−29,45,49,50] In this study, the DIA approach was used for the first time to detect more than 3000 proteins on a mouse model, giving us a more thorough picture of how proteins change over time. Digestive enzyme activation has been demonstrated to be a crucial and early event in the pathogenesis of AP. For example, Amy2, Pnliprp1, Pnliprp2, Pnlip, Cel, Colipase, Prss2, chymotrypsinogen B (Ctrb1), chymotrypsin-like elastase, Cela2a, and Cele3b showed a continuously rising trend that coincided with previous time-course digestive enzymes changes in a necrosis AP model.[29] However, the elevated levels of digestive enzymes were not universal, and decreased levels were also reported in single-time point animal models.[27,28]

The acinar cell currently has defense mechanisms in place to prevent the impacts of digesting proteases. Except for leukocyte elastase inhibitors Serpinb1a and Serpinb1c, the majority of SPIs, such as Serpina3k, Spink1, Serpina1a, Serpina1b, Serpina1e, Serpina3n, and Serpini2, demonstrated an overall increasing trend (Figure S4A). This phenomenon was mostly the same as the previous mild and severe AP model studies. A twice-injected CER-AP rat was shown to have elevated Serpinb6 and Serpina3l in García-Hernández's early proteomic study.[32] In a recent work by García-Hernández et al.,[31] the early phase of CER-AP was studied using TMT-6 plex labeling shotgun proteomics, which identified 997 proteins and 353 differently expressed proteins therefrom. Overexpressed Serpina3k, Serping1, and underexpressed Serpinb1a were found. Unsurprisingly, higher Serpina3k, 3l, and 3n levels were seen in NaT-AP together with lower levels of leukocyte elastase inhibitor A.[29] SPIs are a superfamily of conserved proteins able to inhibit the enzymatic activity of serine proteases and play a major role in complement activation, blood coagulation, inflammation, and fibrinolysis.[51] Clade A serpins include A1 and A3, which are related to inflammatory response, and Serpinb1, which regulates the activity of neutrophil elastase, cathepsin G, and proteinase 3. Overexpression of clade A and underexpression of clade B might indicate protease inhibition and a reduction in the severity of the AP course.

Three different types of filaments make up the cytoskeleton: microfilaments (actin), microtubules (tubulin), and intermediate filaments (keratins).[52] A boost in trend was also seen for proteins including actin, cytoplasmic 1 (Actb), Actg1, tubulin alpha-4A chain (Tuba4a), type II cytoskeletal 8 (Krt8), Krt18, Krt 6a, and Krt 19 (Figure S4B). Actins are highly conserved proteins that are involved in various types of cell motility and are ubiquitously expressed in all eukaryotic cells.[53] Tubulin is the major constituent of microtubules, and alpha-tubulins and beta-tubulins are among the most highly conserved eukaryotic proteins.[54] A group of beta-actin, actin-binding proteins showed increased ratios in response to NaT within 18 h.[29] Elevated levels of actin were also reported in two injections (10

μg/kg) of CER at 5 h after the last injections.[26] Conversely, a decrease of actin, tubulin, and vinculin was found at 2 h after the first injection of CER (twice, 20 μg).[31] This inconsistent observation might be attributed to their participation in secretion in different stages. Keratins are the intermediate filaments of epithelial cells and exist as obligate noncovalent heteropolymers with a minimum of one type-I keratin (K9 to K20) and one type-II keratin (K1 to K8).[55] Excessive overexpression of keratins alters zymogen granule organization and causes aging-associated exocrine atrophy.[56] This corroborates our investigation and previous evidence[56,57] that keratin levels are completely increased after CER stimulation. Additionally, HSPs as cellular stress machinery showed protection in the AP course.[58] In mammals, the major families of HSPs are HSP90, HSP70, HSP60, HSP40, and the small HSPs, wherein four members of the 70 kDa family have been identified-mitochondrial HSP70, Bip, HSP70 (the only inducible form of this family), and HSC70 (constitutive form). HSP70 therapy as a preventative measure prevented trypsinogen activation and the production of trypsinogen activation peptide.[59] In this investigation, four HSP 70s, including Bip, with rising propensity were found, suggesting that these model animals had been acting to defend themselves after a stress response (Figure S4C).

Altered proteins involved in lipid metabolism and temporal lipidomics profiling are highlights of this study. Integrating proteomics and lipidomics further provided a more profound understanding of the lipid change law after the onset of AP. Lipid disorder is not only the etiology of AP but also the result of inflammatory injury.[44,60] Lipoproteins, especially serum HDL, Apoa1, and the ratio of apolipoprotein B to Apoa1 at admission, have been addressed to predict SAP.[41,61−64] Aside from transporting excessive cholesterol from extra-hepatic tissues to the liver, Apoa1 can attenuate lipopolysaccharide-induced cytokine secretion and therefore even downregulate hepatic synthesis of HDL and Apoa1.[41,65] Apoc3 plays an important role in lipid metabolism specifically in regulating the metabolism of triglyceride-rich lipoproteins.[66] It could be hypothesized that the increment in protein abundance of Apoa1, Apoa2, and Apoc3 in the pancreas after CER injections contributed to altered transport and regulation of lipid metabolism and even inflammation. Although accumulated evidence indicated that excessive release of lipase could disturb glycerides or glycerophospholipids,[67] a direct relationship between in situ lipid profiling of the pancreas and AP has not yet been established. Pnlip, Pnliprp1, Pnliprp2, and Pla2 are known to hydrolyze TAGs and phosphoglycerates, which are designed to liberate DAG, MAG, lysophosphoglycerates, and FAs. Accordingly, obvious hydrolysis of TAGs with saturated fatty acid chain happened during the first 7 h before the inflammation peak, and a part of DAG gradually increased at the early stage. In contrast, TAG with polyunsaturated carbon chain elevated first and then returned. All the detected MAG showed a reduced tendency along all the time points, indicating its mobilization for glyceride synthesis or fatty acid liberation. During the course of CER-AP, there are considerable alterations in phosphoglycerides abundance. In particular, some PGs increased significantly from 0 to 12 h and some PAs, PSs, PIs and PCs continued to reduce during the whole period. Similarly, the hydrolysis of phosphoglycerides or MAG may have caused the rise in unsaturated FFAs that we saw, rather than the hydrolysis of triglycerides. This needs further validation.

Additionally, it was surprisingly that the majority of altered proteins revealed by KEGG that are involved in energy metabolism and amino acid metabolism showed a pattern of pullback after growing at the inflammatory peak, which was different from the prior proteomics findings.[25,29,31] For example, prior proteomics studies on the CER-induced AP rat model found that important enzymes involved in the TCA cycle, glycolysis, or BCAA metabolism were reduced.[31] Based on a rat model of SAP, decreased oxidative phosphorylation, carbon metabolism, and degradation of valine, leucine, and isoleucine were also observed.[25] This heterogeneity needed to be further demonstrated and compared. As discussed in our previous AP metabolomics review,[16] increased energy demand and reduced ATP levels have been proposed during AP. While raised BCAA catabolites as precursors entering into the TCA cycle were detected in our previous study as well.[17] In our metabolomics study,[17] the 128 targeted metabolites from the pancreas were classified into five clusters using Mfuzz analysis in time-course CER-AP. Except for cluster 5, all the clusters showed an increasing tendency with a distinct peak, indicating an enhanced metabolism. The glycolysis was centered on clusters 2 and 4, the TCA cycle was associated with clusters 1, 3, and 5, and the valine, leucine, and isoleucine degradation were primarily enriched in clusters 3 and 4. The up-regulation of energy metabolism pathways in the AP edema model may be a self-protective mechanism because BCAA deficiency in the diet made it difficult for animals to maintain pancreatic enzyme activities and BCAA-deficient animals were less able to recover pancreatic enzyme activity after a 23 h fast.[68] It was therefore fairly difficult to surmise that the energy metabolism was increased generally on the mild AP model. However, this did not completely rule out the impact of each specific blocked enzyme and the sampling time point.

Several limitations of this study should be considered. First, since it is difficult to characterize and definite high-abundance proteins in tissues, we ran additional enrichment analysis after deleting 25 proteins (Table S13) with relative high intensities and found that lipid metabolism-related proteins are still crucial (Figure S5). However, the coverage of pancreatic proteins still needs to be enlarged by fractionation owing to a large number of high-abundance proteins such as digestive enzymes and constituent components that were detected and calculated as differentiated markers. Second, since the exact double bond position in the fatty acyls has not been elucidated in this study, more intensive methods development for targeted TAGs, PCs, PIs, and FFAs and subsequent functional analyses are warranted. Third, given that multi-omics performed on an AP mice model or patient is lacking, we anticipated that the picture of interlinked genomic, transcriptomic, proteomic, post-translational, and metabolic relationships would be fleshed out on biofluid or pancreas after an elaborate experimental design.

CONCLUSIONS

In summary, by relative-quantifying the abundance of 3803 proteins within the pancreas of a time-course CER-AP mouse model, we illuminated dynamic trends for various digestive enzymes and adaptive proteins responses to stimulation. These proteome adjustments included increments in anti-trypsin and apolipoproteins as well as up-regulated energy-metabolic enzymes. Furthermore, enhanced lipid transport, regulation, and metabolism were observed, which led to a comprehensive lipidomic profile depiction in pancreas subsequently. Ob-

viously changed phosphoglycerides and polyunsaturated fatty acyls are probably going to play an important role in the pathogenesis of AP. In addition to these newly identified metabolic insights, the integrated omics analyses first provide a comprehensive perspective on AP study.

■ ASSOCIATED CONTENT

ⓈI Supporting Information

The Supporting Information is available free of charge at https://pubs.acs.org/doi/10.1021/acsomega.3c00019.

> Severity indices of CER-induced AP in mice; upset plot showing overlapping proteins in 30 GO terms; relationships between AP dysregulated proteins and KEGG pathways (top 10); relative expressions of SPIs, filaments, and HSP 70s; enrichment analysis of 306 proteins that were screened by time-course analysis after the removal of greater abundances proteins; mass list of DIA windows; and list of 25 proteins with intensity average ($\log_{10}$) larger than 6 (PDF)

> Detailed mass spectrometer parameters of MRM transitions for lipidomics; relative quantification data of 3803 proteins by DIA; list of 171 proteins screened by time-course analysis; GO enrichment analysis of 171 proteins; information of 44 proteins involved in top 10 terms in GO classification; enriched pathways of 171 proteins by KEGG pathway analysis; annotation of 16 proteins involved in lipids metabolism and signaling pathway; QC sample data for lipidomics of pancreatic tissue; total lipids in both positive and negative modes; cluster data of 1364 lipids by Mfuzz clustering analysis; and annotation of 22 proteins involved in metabolic pathways (ZIP)

■ AUTHOR INFORMATION

Corresponding Author

Dan Du − *West China Centre of Excellence for Pancreatitis, Institute of Integrated Traditional Chinese and Western Medicine, Sichuan Provincial Pancreatitis Centre and West China-Liverpool Biomedical Research Centre, West China Hospital/West China Medical School, Sichuan University, Chengdu 610041, China;* ⓞ orcid.org/0000-0001-9745-8197; Email: dudan1520@163.com

Authors

Rui Wang − *West China Centre of Excellence for Pancreatitis, Institute of Integrated Traditional Chinese and Western Medicine, Sichuan Provincial Pancreatitis Centre and West China-Liverpool Biomedical Research Centre, West China Hospital/West China Medical School, Sichuan University, Chengdu 610041, China; Advanced Mass Spectrometry Center, Research Core Facility, Frontiers Science Center for Disease-Related Molecular Network, West China Hospital, Sichuan University, Chengdu 610041, China*

Yiqin Wang − *West China Centre of Excellence for Pancreatitis, Institute of Integrated Traditional Chinese and Western Medicine, Sichuan Provincial Pancreatitis Centre and West China-Liverpool Biomedical Research Centre, West China Hospital/West China Medical School, Sichuan University, Chengdu 610041, China*

Yiran Tao − *West China-California Research Center for Predictive Intervention Medicine, West China Hospital, Sichuan University, Chengdu 610041, China*

Liqiang Hu − *Advanced Mass Spectrometry Center, Research Core Facility, Frontiers Science Center for Disease-Related Molecular Network, West China Hospital, Sichuan University, Chengdu 610041, China*

Qi Qiu − *West China Centre of Excellence for Pancreatitis, Institute of Integrated Traditional Chinese and Western Medicine, Sichuan Provincial Pancreatitis Centre and West China-Liverpool Biomedical Research Centre, West China Hospital/West China Medical School, Sichuan University, Chengdu 610041, China*

Qianlun Pu − *Advanced Mass Spectrometry Center, Research Core Facility, Frontiers Science Center for Disease-Related Molecular Network, West China Hospital, Sichuan University, Chengdu 610041, China*

Juqin Yang − *Biobank, West China Hospital, Sichuan University, Chengdu 610041, China*

Shisheng Wang − *Proteomics-Metabolomics Platform of Core Facilities, West China Hospital, Sichuan University, Chengdu 610041, China*

Yan Huang − *West China Centre of Excellence for Pancreatitis, Institute of Integrated Traditional Chinese and Western Medicine, Sichuan Provincial Pancreatitis Centre and West China-Liverpool Biomedical Research Centre, West China Hospital/West China Medical School, Sichuan University, Chengdu 610041, China*

Xiaoting Chen − *Animal Experimental Center, West China Hospital, Sichuan University, Chengdu 610041, China*

Ping Zhu − *West China Centre of Excellence for Pancreatitis, Institute of Integrated Traditional Chinese and Western Medicine, Sichuan Provincial Pancreatitis Centre and West China-Liverpool Biomedical Research Centre, West China Hospital/West China Medical School, Sichuan University, Chengdu 610041, China*

Hao Yang − *Proteomics-Metabolomics Platform of Core Facilities, West China Hospital, Sichuan University, Chengdu 610041, China;* orcid.org/0000-0003-2214-9474

Qing Xia − *West China Centre of Excellence for Pancreatitis, Institute of Integrated Traditional Chinese and Western Medicine, Sichuan Provincial Pancreatitis Centre and West China-Liverpool Biomedical Research Centre, West China Hospital/West China Medical School, Sichuan University, Chengdu 610041, China*

Complete contact information is available at:
https://pubs.acs.org/10.1021/acsomega.3c00019

Author Contributions

D.D. conceptualization; R.W., Y.W., Q.P., and J.Y. methodology; R.W. software; R.W. and Q.P. data acquisition; R.W. and Q.P. data curation; L.H., Y.H., X.C., and P.Z., investigation; R.W., Q.Q., and D.D. formal analysis; R.W., Y.T., and D.D. writing-reviewing and editing; S.W., H.Y., Q.X., and D.D. supervision; Q.X. and D.D. funding acquisition; and Q.X. and D.D. resources.

Notes

The authors declare no competing financial interest.

The mass spectrometry proteomics data have been deposited to the ProteomeXchange Consortium via the iProX partner repository with the data set identifier PXD03567. The data sets supporting the conclusions of this article are available in the publicly available repositories.

■ ABBREVIATIONS

AP	acute pancreatitis
HTG	alcohol and hypertriglyceridemia
ER	endoplasmic reticulum
CER	cerulein
DIA-MS	data-independent acquisition mass spectrometry
HE	hematoxylin and eosin
RT	retention time
DDA	data-dependent acquisition
AGC	automatic gain control
NCE	normalized collision energy
DIA	data-independent acquisition
MRM	multiple reaction monitoring
FDR	false discovery rate
KNN	k-nearest neighbor
HCA	hierarchical clustering analysis
GO	Gene Ontology
BP	biological process
CC	cellular component
MF	molecular function
KEGG	Kyoto encyclopedia of genes and genomes
PCA	principle component analysis
PPI	protein−protein interaction
TAGs	triacylglycerols
PEs	phosphatidylethanolamines
PGs	phosphatidylglycerols
CEs	cholesteryl esters
PCs	phosphatidylcholines
Cers	ceramides
GlcCERs	glucosylceramides
LacCERs	lactosylceramides
SMs	sphingomyelins
DAGs	diacylglycerols
MAGs	monoacylglycerols
LPCs	lysophosphatidylcholines
LPEs	lysophosphatidylethanolamines
LPGs	lysophosphatidylglycerols
LPIs	lysophosphatidylinositols
PIs	phosphatidylinositols
PS	phosphatidylserine
CLs	cardiolipins
PAs	phosphatidic acid
FFAs	free fatty acids
EPA	eicosapentaenoic acid
SPIs	serine protease inhibitors
HSPs	heat shock proteins

■ REFERENCES

(1) Boxhoorn, L.; Voermans, R. P.; Bouwense, S. A.; Bruno, M. J.; Verdonk, R. C.; Boermeester, M. A.; van Santvoort, H. C.; Besselink, M. G. Acute pancreatitis. *Lancet* **2020**, *396*, 726−734.

(2) Lee, P. J.; Papachristou, G. I. New insights into acute pancreatitis. *Nat. Rev. Gastroenterol. Hepatol.* **2019**, *16*, 479−496.

(3) Logsdon, C. D.; Ji, B. The role of protein synthesis and digestive enzymes in acinar cell injury. *Nat. Rev. Gastroenterol. Hepatol.* **2013**, *10*, 362−370.

(4) Huang, W.; Cane, M. C.; Mukherjee, R.; Szatmary, P.; Zhang, X.; Elliott, V.; Ouyang, Y.; Chvanov, M.; Latawiec, D.; Wen, L.; et al. Caffeine protects against experimental acute pancreatitis by inhibition of inositol 1,4,5-trisphosphate receptor-mediated Ca^{2+} release. *Gut* **2017**, *66*, 301−313.

(5) Saluja, A.; Dudeja, V.; Dawra, R.; Sah, R. P. Early Intra-Acinar Events in Pathogenesis of Pancreatitis. *Gastroenterology* **2019**, *156*, 1979−1993.

(6) Gukovskaya, A. S.; Gukovsky, I.; Algül, H.; Habtezion, A. Autophagy, Inflammation, and Immune Dysfunction in the Pathogenesis of Pancreatitis. *Gastroenterology* **2017**, *153*, 1212−1226.

(7) Biczo, G.; Vegh, E. T.; Shalbueva, N.; Mareninova, O. A.; Elperin, J.; Lotshaw, E.; Gretler, S.; Lugea, A.; Malla, S. R.; Dawson, D.; et al. Mitochondrial Dysfunction, Through Impaired Autophagy, Leads to Endoplasmic Reticulum Stress, Deregulated Lipid Metabolism, and Pancreatitis in Animal Models. *Gastroenterology* **2018**, *154*, 689−703.

(8) Wen, L.; Voronina, S.; Javed, M. A.; Awais, M.; Szatmary, P.; Latawiec, D.; Chvanov, M.; Collier, D.; Huang, W.; Barrett, J.; et al. Inhibitors of ORAI1 Prevent Cytosolic Calcium-Associated Injury of Human Pancreatic Acinar Cells and Acute Pancreatitis in 3 Mouse Models. *Gastroenterology* **2015**, *149*, 481−492.

(9) Javed, M. A.; Wen, L.; Awais, M.; Latawiec, D.; Huang, W.; Chvanov, M.; Schaller, S.; Bordet, T.; Michaud, M.; Pruss, R.; et al. TRO40303 Ameliorates Alcohol-Induced Pancreatitis Through Reduction of Fatty Acid Ethyl Ester-Induced Mitochondrial Injury and Necrotic Cell Death. *Pancreas* **2018**, *47*, 18−24.

(10) Long, N. P.; Nghi, T. D.; Kang, Y. P.; Anh, N. H.; Kim, H. M.; Park, S. K.; Kwon, S. W. Toward a Standardized Strategy of Clinical Metabolomics for the Advancement of Precision Medicine. *Metabolites* **2020**, *10*, 51.

(11) Mukherjee, R.; Nunes, Q.; Huang, W.; Sutton, R. Precision medicine for acute pancreatitis: current status and future opportunities. *Precis. Clin. Med.* **2019**, *2*, 81−86.

(12) Mederos, M. A.; Reber, H. A.; Girgis, M. D. Acute Pancreatitis. *JAMA* **2021**, *325*, 382−390.

(13) Huang, J. H.; He, D.; Chen, L.; Dong, C. Y.; Zhang, S. H.; Qin, Y. H.; Yu, R.; Ahmed, R.; Kuang, J. J.; Zhang, X. W. GC-MS based metabolomics strategy to distinguish three types of acute pancreatitis. *Pancreatology* **2019**, *19*, 630−637.

(14) van den Berg, F. F.; van Dalen, D.; Hyoju, S. K.; van Santvoort, H. C.; Besselink, M. G.; Wiersinga, W. J.; Zaborina, O.; Boermeester, M. A.; Alverdy, J. Western-type diet influences mortality from necrotising pancreatitis and demonstrates a central role for butyrate. *Gut* **2021**, *70*, 915−927.

(15) Villaseñor, A.; Kinross, J. M.; Li, J. V.; Penney, N.; Barton, R. H.; Nicholson, J. K.; Darzi, A.; Barbas, C.; Holmes, E. 1H NMR global metabolic phenotyping of acute pancreatitis in the emergency unit. *J. Proteome Res.* **2014**, *13*, 5362−5375.

(16) Peng, Y.; Hong, J.; Raftery, D.; Xia, Q.; Du, D. Metabolomic-based clinical studies and murine models for acute pancreatitis disease: A review. *Biochim. Biophys. Acta, Mol. Basis Dis.* **2021**, *1867*, 166123.

(17) Huang, Y.; Wen, Y.; Wang, R.; Hu, L.; Yang, J.; Yang, J.; Pu, Q.; Han, C.; Cai, W.; Peng, Y.; et al. Temporal metabolic trajectory analyzed by LC-MS/MS based targeted metabolomics in acute pancreatitis pathogenesis and Chaiqin Chengqi decoction therapy. *Phytomedicine* **2022**, *99*, 153996.

(18) Barreto, S. G.; Habtezion, A.; Gukovskaya, A.; Lugea, A.; Jeon, C.; Yadav, D.; Hegyi, P.; Venglovecz, V.; Sutton, R.; Pandol, S. J. Critical thresholds: key to unlocking the door to the prevention and specific treatments for acute pancreatitis. *Gut* **2021**, *70*, 194−203.

(19) Lippi, G.; Valentino, M.; Cervellin, G. Laboratory diagnosis of acute pancreatitis: in search of the Holy Grail. *Crit. Rev. Clin. Lab. Sci.* **2012**, *49*, 18−31.

(20) Waldron, R. T.; Lugea, A.; Gulla, A.; Pandol, S. J. Proteomic Identification of Novel Plasma Biomarkers and Pathobiologic Pathways in Alcoholic Acute Pancreatitis. *Front Physiol.* **2018**, *9*, 1215.

(21) Nunes, Q. M.; Su, D.; Brownridge, P. J.; Simpson, D. M.; Sun, C.; Li, Y.; Bui, T. P.; Zhang, X.; Huang, W.; Rigden, D. J.; et al. The heparin-binding proteome in normal pancreas and murine experimental acute pancreatitis. *PLoS One* **2019**, *14*, No. e0217633.

(22) Tan, J. H.; Cao, R. C.; Zhou, L.; Zhou, Z. T.; Chen, H. J.; Xu, J.; Chen, X. M.; Jin, Y. C.; Lin, J. Y.; Qi, Z. C.; et al. EMC6 regulates acinar apoptosis via APAF1 in acute and chronic pancreatitis. *Cell Death Dis.* **2020**, *11*, 966.

(23) Cruz-Monserrate, Z.; Gumpper, K.; Pita, V.; Hart, P. A.; Forsmark, C.; Whitcomb, D. C.; Yadav, D.; Waldron, R. T.; Pandol, S.; Steen, H.; et al. Biomarkers of Chronic Pancreatitis: A systematic literature review. *Pancreatology* **2021**, *21*, 323−333.

(24) Li, H.; Xu, Y.; Zhou, X.; Jin, T.; Wang, Z.; Sun, Y.; Wang, H.; Jiang, D.; Yin, C.; Shen, B.; et al. DIA-Based Proteomic Analysis of Plasma Protein Profiles in Patients with Severe Acute Pancreatitis. *Molecules* **2022**, *27*, 3880.

(25) Wang, C.; Zhang, Y.; Tan, J.; Chen, B.; Sun, L. Improved Integrated Whole Proteomic and Phosphoproteomic Profiles of Severe Acute Pancreatitis. *J. Proteome Res.* **2020**, *19*, 2471−2482.

(26) Fétaud, V.; Frossard, J. L.; Farina, A.; Pastor, C. M.; Bühler, L.; Dumonceau, J. M.; Hadengue, A.; Hochstrasser, D. F.; Lescuyer, P. Proteomic profiling in an animal model of acute pancreatitis. *Proteomics* **2008**, *8*, 3621−3631.

(27) Chen, X.; Sans, M. D.; Strahler, J. R.; Karnovsky, A.; Ernst, S. A.; Michailidis, G.; Andrews, P. C.; Williams, J. A. Quantitative organellar proteomics analysis of rough endoplasmic reticulum from normal and acute pancreatitis rat pancreas. *J. Proteome Res.* **2010**, *9*, 885−896.

(28) Fétaud-Lapierre, V.; Pastor, C. M.; Farina, A.; Hochstrasser, D. F.; Frossard, J. L.; Lescuyer, P. Proteomic analysis of heat shock-induced protection in acute pancreatitis. *J. Proteome Res.* **2010**, *9*, 5929−5942.

(29) Fétaud-Lapierre, V.; Pastor, C. M.; Jorge-Costa, M.; Hochstrasser, D. F.; Morel, D. R.; Frossard, J. L.; Lescuyer, P. Time-course proteomic analysis of taurocholate-induced necrotizing acute pancreatitis. *J. Proteomics* **2013**, *85*, 12−27.

(30) Shapiro, J. P.; Komar, H. M.; Hancioglu, B.; Yu, L.; Jin, M.; Ogata, Y.; Hart, P. A.; Cruz-Monserrate, Z.; Lesinski, G. B.; Conwell, D. L. Laser Capture Microdissection of Pancreatic Acinar Cells to Identify Proteomic Alterations in a Murine Model of Caerulein-Induced Pancreatitis. *Clin. Transl. Gastroenterol.* **2017**, *8*, No. e89.

(31) García-Hernández, V.; Sánchez-Bernal, C.; Schvartz, D.; Calvo, J. J.; Sanchez, J. C.; Sánchez-Yagüe, J. A tandem mass tag (TMT) proteomic analysis during the early phase of experimental pancreatitis reveals new insights in the disease pathogenesis. *J. Proteomics* **2018**, *181*, 190−200.

(32) García-Hernández, V.; Sánchez-Bernal, C.; Sarmiento, N.; Viana, R. A.; Ferreira, L.; Pérez, N.; Calvo, J. J.; Sánchez-Yagüe, J. Proteomic analysis of the soluble and the lysosomal+mitochondrial fractions from rat pancreas: Implications for cerulein-induced acute pancreatitis. *Biochim. Biophys. Acta* **2012**, *1824*, 1058−1067.

(33) Fahy, E.; Subramaniam, S.; Brown, H. A.; Glass, C. K.; Merrill, A. H., Jr.; Murphy, R. C.; Raetz, C. R.; Russell, D. W.; Seyama, Y.; Shaw, W.; et al. A comprehensive classification system for lipids. *J. Lipid Res.* **2005**, *46*, 839−861.

(34) Huang, W.; Booth, D. M.; Cane, M. C.; Chvanov, M.; Javed, M. A.; Elliott, V. L.; Armstrong, J. A.; Dingsdale, H.; Cash, N.; Li, Y.; et al. Fatty acid ethyl ester synthase inhibition ameliorates ethanol-induced Ca^{2+}-dependent mitochondrial dysfunction and acute pancreatitis. *Gut* **2014**, *63*, 1313−1324.

(35) Doerr, A. DIA mass spectrometry. *Nat. Methods* **2014**, *12*, 35.

(36) Hu, A.; Noble, W. S.; Wolf-Yadlin, A. Technical advances in proteomics: new developments in data-independent acquisition. *F1000Res.* **2016**, *5*, 419.

(37) Krasny, L.; Huang, P. H. Data-independent acquisition mass spectrometry (DIA-MS) for proteomic applications in oncology. *Mol. Omics* **2021**, *17*, 29–42.

(38) Castro-Perez, J. M.; Kamphorst, J.; DeGroot, J.; Lafeber, F.; Goshawk, J.; Yu, K.; Shockcor, J. P.; Vreeken, R. J.; Hankemeier, T. Comprehensive LC–MSE Lipidomic Analysis using a Shotgun Approach and Its Application to Biomarker Detection and Identification in Osteoarthritis Patients. *J. Proteome Res.* **2010**, *9*, 2377–2389.

(39) Zhang, F.; Ge, W.; Ruan, G.; Cai, X.; Guo, T. Data-Independent Acquisition Mass Spectrometry-Based Proteomics and Software Tools: A Glimpse in 2020. *Proteomics* **2020**, *20*, No. e1900276.

(40) Mangaraj, M.; Nanda, R.; Panda, S. A.-I. Apolipoprotein A-I: A Molecule of Diverse Function. *Indian J. Clin. Biochem.* **2016**, *31*, 253–259.

(41) Peng, Y. S.; Chen, Y. C.; Tian, Y. C.; Yang, C. W.; Lien, J. M.; Fang, J. T.; Wu, C. S.; Hung, C. F.; Hwang, T. L.; Tsai, Y. H.; et al. Serum levels of apolipoprotein A-I and high-density lipoprotein can predict organ failure in acute pancreatitis. *Crit. Care* **2015**, *19*, 88.

(42) Pretis, N.; Amodio, A.; Frulloni, L. Hypertriglyceridemic pancreatitis: Epidemiology, pathophysiology and clinical management. *United Eur. Gastroenterol. J.* **2018**, *6*, 649–655.

(43) Scherer, J.; Singh, V. P.; Pitchumoni, C. S.; Yadav, D. Issues in Hypertriglyceridemic Pancreatitis. *J. Clin. Gastroenterol.* **2014**, *48*, 195–203.

(44) Guo, Y. Y.; Li, H. X.; Zhang, Y.; He, W. H. Hyper-triglyceridemia-induced acute pancreatitis: progress on disease mechanisms and treatment modalities. *Discov. Med.* **2019**, *27*, 101–109.

(45) Yu, J. H.; Yun, S. Y.; Lim, J. W.; Kim, H.; Kim, K. H. Proteome analysis of rat pancreatic acinar cells: implication for cerulein-induced acute pancreatitis. *Proteomics* **2003**, *3*, 2446–2453.

(46) Paulo, J. A.; Urrutia, R.; Banks, P. A.; Conwell, D. L.; Steen, H. Proteomic analysis of a rat pancreatic stellate cell line using liquid chromatography tandem mass spectrometry (LC-MS/MS). *J. Proteomics* **2011**, *75*, 708–717.

(47) Paulo, J. A.; Urrutia, R.; Banks, P. A.; Conwell, D. L.; Steen, H. Proteomic analysis of an immortalized mouse pancreatic stellate cell line identifies differentially-expressed proteins in activated vs non-proliferating cell states. *J. Proteome Res.* **2011**, *10*, 4835–4844.

(48) Hong, X.; Zhang, Q.; Wang, D.; Xia, S.; Wang, G.; Zhang, G.; Chen, H.; Wu, Y.; Dong, S. iTRAQ-based quantitative proteomic analysis for identification of biomarkers associated with emodin against severe acute pancreatitis in rats. *RSC Adv.* **2016**, *6*, 72447–72457.

(49) Papachristou, G. I.; Malehorn, D. E.; Lamb, J.; Slivka, A.; Bigbee, W. L.; Whitcomb, D. C. Serum proteomic patterns as a predictor of severity in acute pancreatitis. *Pancreatology* **2007**, *7*, 317–324.

(50) Zhang, W.; Zhao, Y.; Zeng, Y.; Yu, X.; Yao, J.; Zhao, S.; Bao, Z.; Chen, J.; Wang, X. Hyperlipidemic Versus Normal-Lipid Acute Necrotic Pancreatitis. *Pancreas* **2012**, *41*, 317–322.

(51) Khan, M. S.; Singh, P.; Azhar, A.; Naseem, A.; Rashid, Q.; Kabir, M. A.; Jairajpuri, M. A. Serpin Inhibition Mechanism: A Delicate Balance between Native Metastable State and Polymerization. *J. Amino Acids* **2011**, *2011*, 606797.

(52) De Lisle, R. C. Role of the actin cytoskeleton in acinar cell protein secretion. In *Pancreapedia: Exocrine Pancreas Knowledge Base*; Michigan Publishing, 2020.

(53) Dominguez, R.; Holmes, K. C. Actin structure and function. *Annu. Rev. Biophys.* **2011**, *40*, 169–186.

(54) Wade, R. H. Microtubules. *Methods Mol. Med.* **2007**, *137*, 1–16.

(55) Zhou, Q.; Toivola, D. M.; Feng, N.; Greenberg, H. B.; Franke, W. W.; Omary, M. B. Keratin 20 helps maintain intermediate filament organization in intestinal epithelia. *Mol. Biol. Cell* **2003**, *14*, 2959–2971.

(56) Toivola, D. M.; Nakamichi, I.; Strnad, P.; Michie, S. A.; Ghori, N.; Harada, M.; Zeh, K.; Oshima, R. G.; Baribault, H.; Omary, M. B. Keratin overexpression levels correlate with the extent of spontaneous pancreatic injury. *Am. J. Pathol.* **2008**, *172*, 882–892.

(57) Zhong, B.; Zhou, Q.; Toivola, D. M.; Tao, G. Z.; Resurreccion, E. Z.; Omary, M. B. Organ-specific stress induces mouse pancreatic keratin overexpression in association with NF-kappaB activation. *J. Cell Sci.* **2004**, *117*, 1709–1719.

(58) Saluja, A.; Dudeja, V. Heat shock proteins in pancreatic diseases. *J. Gastroenterol. Hepatol.* **2008**, *23*, S42–S45.

(59) Frossard, J. L.; Bhagat, L.; Lee, H. S.; Hietaranta, A. J.; Singh, V. P.; Song, A. M.; Steer, M. L.; Saluja, A. K. Both thermal and non-thermal stress protect against caerulein induced pancreatitis and prevent trypsinogen activation in the pancreas. *Gut* **2002**, *50*, 78–83.

(60) Vonlaufen, A.; Wilson, J. S.; Apte, M. V. Molecular mechanisms of pancreatitis: current opinion. *J. Gastroenterol. Hepatol.* **2008**, *23*, 1339–1348.

(61) Khan, J.; Nordback, I.; Sand, J. Serum lipid levels are associated with the severity of acute pancreatitis. *Digestion* **2013**, *87*, 223–228.

(62) Hong, W.; Lin, S.; Zippi, M.; Geng, W.; Stock, S.; Zimmer, V.; Xu, C.; Zhou, M. High-Density Lipoprotein Cholesterol, Blood Urea Nitrogen, and Serum Creatinine Can Predict Severe Acute Pancreatitis. *BioMed Res. Int.* **2017**, *2017*, 1648385.

(63) Zhou, C. L.; Zhang, C. H.; Zhao, X. Y.; Chen, S. H.; Liang, H. J.; Hu, C. L.; Chen, N. W. Early prediction of persistent organ failure by serum apolipoprotein A-I and high-density lipoprotein cholesterol in patients with acute pancreatitis. *Clin. Chim. Acta* **2018**, *476*, 139–145.

(64) Wu, J.; Wang, Y.; Li, H.; Tan, W.; Chen, X.; Ye, S. Serum apolipoprotein B-to-apolipoprotein A1 ratio is independently associated with disease severity in patients with acute pancreatitis. *Sci. Rep.* **2019**, *9*, 7764.

(65) Li, Y.; Dong, J. B.; Wu, M. P. Human ApoA-I overexpression diminishes LPS-induced systemic inflammation and multiple organ damage in mice. *Eur. J. Pharmacol.* **2008**, *590*, 417–422.

(66) Ooi, E. M.; Barrett, P. H.; Chan, D. C.; Watts, G. F. Apolipoprotein C-III: understanding an emerging cardiovascular risk factor. *Clin. Sci.* **2008**, *114*, 611–624.

(67) Zechner, R.; Zimmermann, R.; Eichmann, T. O.; Kohlwein, S. D.; Haemmerle, G.; Lass, A.; Madeo, F. FAT SIGNALS - Lipases and Lipolysis in Lipid Metabolism and Signaling. *Cell Metab.* **2012**, *15*, 279–291.

(68) Lyman, R. L.; Wilcox, S. S. Effect of Acute Amino Acid Deficiencies on Carcass Composition and Pancreatic Function in the Force-fed Rat. *J. Nutr.* **1963**, *79*, 37–44.